European Journal of Pharmaceutics and Biopharmaceutics 77 (2011) 360–367

Contents lists available at ScienceDirect

European Journal of Pharmaceutics and Biopharmaceutics

journal homepage: www.elsevier.com/locate/ejpb

Research paper

Internal benchmarking of a human blood–brain barrier cell model for screening of nanoparticle uptake and transcytosis

Michelle Nic Ragnaill [a,*], Meredith Brown [a,b], Dong Ye [a], Mattia Bramini [a], Sean Callanan [b], Iseult Lynch [a], Kenneth A. Dawson [a]

[a] School of Chemistry & Chemical Biology, and UCD Conway Institute, University College Dublin, Dublin, Ireland
[b] School of Agriculture, Food Science & Veterinary Medicine, University College Dublin, Dublin, Ireland

ARTICLE INFO

Article history:
Available online 12 January 2011

Keywords:
Blood–brain barrier
Nanoparticles
Transcytosis
Bionanointeraction

ABSTRACT

Transport of drugs across the blood–brain barrier, which protects the brain from harmful agents, is considered the holy grail of targeted delivery, due to the extreme effectiveness of this barrier at preventing passage of non-essential molecules through to the brain. This has caused severe limitations for therapeutics for many brain-associated diseases, such as HIV and neurodegenerative diseases. Nanomaterials, as a result of their small size (in the order of many protein–lipid clusters routinely transported by cells) and their large surface area (which acts as a scaffold for proteins thereby rendering nanoparticles as biological entities) offer great promise for neuro-therapeutics. However, in parallel with developing neuro-therapeutic applications based on nanotechnology, it is essential to ensure their safety and long-term consequences upon reaching the brain. One approach to determining safe application of nanomaterials in biology is to obtain a deep mechanistic understanding of the interactions between nanomaterials and living systems (bionanointeractions). To this end, we report here on the establishment and internal round robin validation of a human cell model of the blood–brain barrier for use as a tool for screening nanoparticles interactions, and assessing the critical nanoscale parameters that determine transcytosis.

1. Introduction

As nanoparticles have, and will increasingly appear, in everyday consumer products, there has been considerable interest in ensuring that these materials are safe and are introduced safely into the market. Applications range from nano-sized titanium dioxide and zinc oxide in sun creams, clay nanoparticles in beer bottles, silver nanoparticles in food storage containers, and nano-hydroxyapatite in tooth paste. Careful and thorough attention to detail both by institutions and researchers in this arena has now begun to prevail, and broadly speaking early fears of great hazard (associated solely with the nanoscale) have declined, being replaced by cautious disciplined efforts to ensure safety. Besides the very evident everyday advantages for consumer products, some of the greatest hopes for bionanoscience involve biomedical applications for new therapies and diagnostic tools for some of the most deadly and intractable human diseases.

The basis of new hope in therapeutics involves several key factors. Firstly, the endogenous biological transport processes are mainly on the scale of some tens of nanometers, and by exploiting them, we have the possibility of the unique access of nanoparticles to hitherto inaccessible disease sites. Secondly, the primary immune system is less active for objects somewhat less than several hundred nanometers, allowing for longer circulation or processing times before clearance. There are clear hopes that a fundamental understanding and control of how the nanoparticle surface is affected [12,14] and read by living organisms will enable major developments in medicine. We should also not forget that pharmaceutical products involving the more basic applications of nanotechnology have already been approved for clinical uses, and there are more than 300 nano-enabled products at various stages of preclinical development [1].

The blood–brain barrier (BBB) is a metabolic and cellular structure in the central nervous system (CNS) that restricts the passage of various chemical substances and foreign materials (including many viruses and bacteria) between the bloodstream and the neural tissue itself, while still allowing the passage of substances essential to metabolic function, from oxygen to various proteins. Tight junctions formed between the endothelial cells, supporting cells (astrocytes, pericytes, and microglia), enzymes, receptors, transporters, and efflux pumps control and limit the access of molecules to the brain [2]. Several methods of transport across the BBB have been identified, including paracellular or transcellular

* Corresponding author. Address: Centre for BioNano Interactions, School of Chemistry & Chemical Biology, and UCD Conway Institute, University College Dublin, Belfield, Dublin 4, Ireland. Tel.: 00353-017166854.
E-mail address: michelle.nicraghnaill@ucd.ie (M.N. Ragnaill).

0939-6411/$ - see front matter © 2011 Elsevier B.V. All rights reserved.
doi:10.1016/j.ejpb.2010.12.024

pathways, transport proteins, receptor-mediated transcytosis, and adsorptive transcytosis (Fig. 1) [2]. The interactions of nanoparticles at the BBB have not yet been thoroughly described, although interest in this arena is rapidly increasing [15–17]. Indeed, nanoparticle binding to apolipoprotein [3,4] has been suggested as a mechanism via which nanoparticles could utilize existing pathways to access the brain.

Although the neuroprotective function is vital, the BBB also impedes the passage of pharmacologically beneficial substances in instances of CNS diseases, such as Alzheimer's disease, Parkinson's disease, neuro-AIDS, stroke and dementia. The BBB permits the transport of only a very limited number of small hydrophobic molecular drugs. Frustratingly, many anti-cancer drugs are large hydrophobic molecules which also activate the MDR (multi-drug resistance) efflux pumps expressed by the BBB. There are a few drugs that are small enough, and have been shown to cross the BBB, namely irinotecan (a topoisomerase I inhibitor), melphalan, and temozolomide. These molecules are less than 80 nm and are thought to penetrate the BBB due to the leaky vessels associated with the primary sites of human brain cancers [5].

While *in vivo* studies of the BBB are not the most transparent methods to study metabolism and transport, this form of testing remains necessary for endpoint validation. Still, there is a major world wide effort to limit the role of animal testing, and in any case where models are available, they have the capacity for greater insight into cellular mechanisms. Several *in vitro* studies have been developed in order to address some of the fundamental mechanisms involved in BBB crossing. The first model consisted of primary brain endothelial monolayers (1980s); however, it is difficult for them to form tight junctions *in vitro*, as evidenced by low TEER (trans-endothelial electrical resistance) measurements. Additionally, the primary cells often lose their typical morphology and cell-specific markers (such as gamma glutyl transpeptidase), reducing their usefulness as a model of the *in vivo* BBB. Improvements to the model consisted of using astrocyte-conditioned media, immortalization of the cells, and co-culture of astrocyte and endothelial cells. Rat cells have been the most commonly used to build primary co-culture models, evidently because of their availability in laboratory-animal settings, and their usefulness in comparison with *in vivo* work, which is often also performed on the rat animal model. A cat co-culture blood–brain barrier model has also been created and validated for use in studying the neurological pathogenesis of feline immunodeficiency virus (FIV), a model for neuro-AIDS [6]. There are two human endothelial cell lines: hCMEC/D3 [7,8] and HBMVE [9], which have been isolated, cultured, and validated, although neither is commercially available. The hCMEC/D3 cell line was chosen as it is the closest available correlate to the human *in vivo* situation, and does not require co-culture with primary astrocyte cells, making it easier to work with for quantitative studies. In addition, the porous transwell system upon which the hCMEC/D3 monolayer was grown, as described in this paper, has previously been utilized in the presence of monolayers from alternate cell lines by other groups [19,20].

In recent years, significant effort has been directed toward mimicking the *in vivo* BBB using immortalized hCMEC/D3 cells. As this cell line can differentiate into a monolayer in culture after 7–10 days, seeding the cells onto a permeable filter, the so-called transwell system (Fig. 2) enables an *in vitro* BBB model to be established. The transwell is composed of an insert filter on which the cell monolayer is grown, and an acceptor well, with the apical chamber mimicking the blood and the basolateral chamber mimicking the brain, as shown in Fig. 2. Thus, molecules loaded into

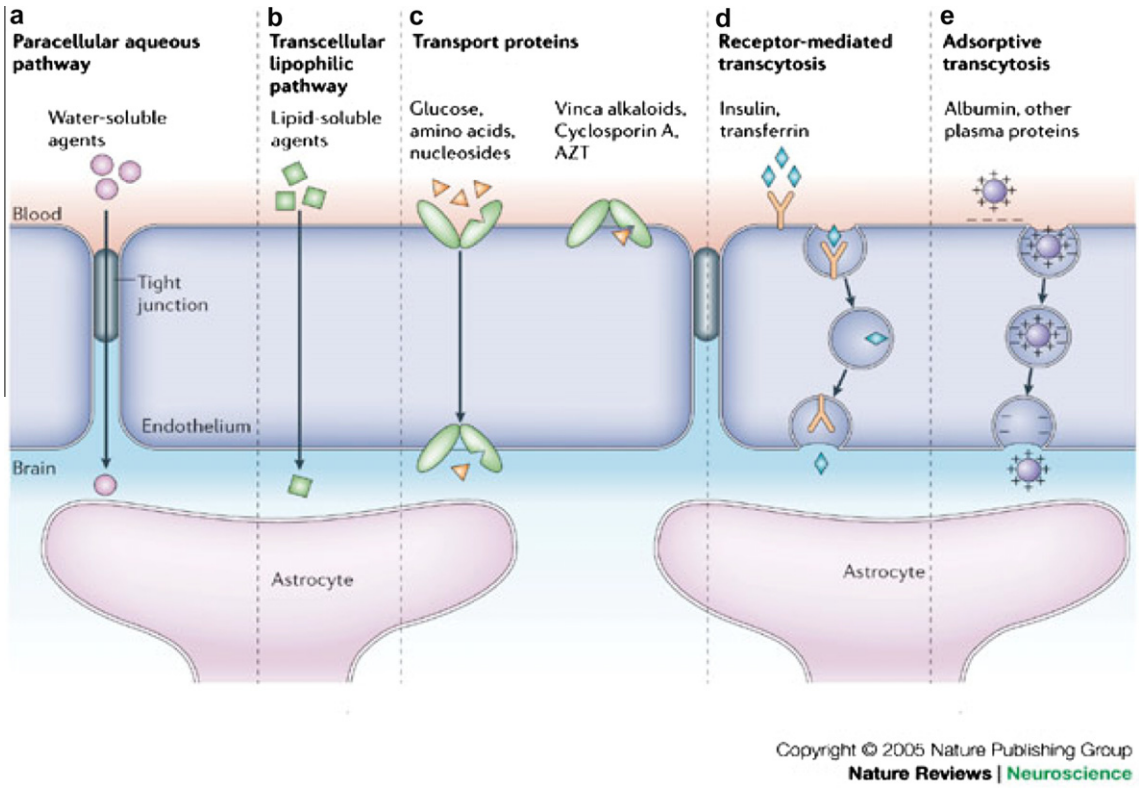

Fig. 1. Pathways across the blood–brain barrier [2]. Size, surface charge, and molecular signaling influence the ability of substances to cross the BBB through these various pathways. (For interpretation of the references to colour in this figure legend, the reader is referred to the web version of this article.)

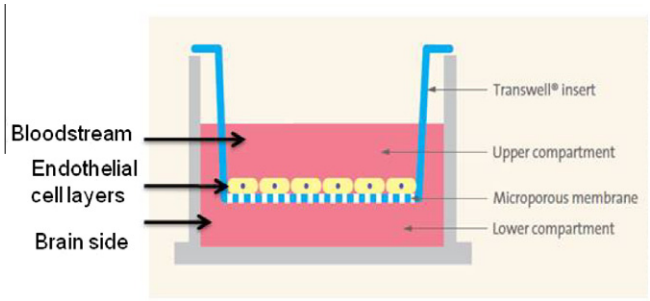

Fig. 2. Schematic of the *in vitro* blood–brain barrier. (For interpretation of the references to colour in this figure legend, the reader is referred to the web version of this article.)

the apical chamber are presented to the cellular barrier formed on the filter, which can then be taken up by the cells by a receptor-mediated (transcytosis) process (Fig. 2).

While it is clearly desirable to apply these established models to study nanoparticle BBB crossing, it transpires that there are very significant challenges in achieving this, specifically gaining reproducible data on nanoparticle flux across the barrier. The difficulties far exceed those compared to molecular applications of these models, and we feel it is useful to discuss them at some length based on extensive experience in this area. For example, interaction of the NPs with the filter material, including potential for blocking of the pores are complicated issues.

It should also be recognized that extraction of the cell-barrier transport property from the filter alone requires us to subtract the fluxes from the filter support alone from the flux of the combined *in vitro* BBB model. This requires the flux through the filter to be significantly higher than that of the cell-barrier (and the combination) otherwise one must determine a small flux from the difference between two large (noisy) fluxes. These issues therefore lay quite a lot of attention on the nature of the filter and its interactions with particles under flow. We should also comment that many of the challenges laid out here are by no means fully resolved, and we continue to explore all aspects of the problem in an effort to produce a truly quantitative and ultimately validatable model. The present paper should be considered a 'status report' on the efforts so far, suggesting the need for considerable advancement.

We have invested significant effort into devising and implementing a robust protocol for establishment of the *in vitro* BBB model, and validating it via an internal benchmarking process. Using hCMEC/D3 cells (immortalized human brain capillary endothelial cells, a gift from Florence Miller, B.B. Weksler, INSERM, France), we report here on the optimization and internal benchmarking validation of an *in vitro* human BBB model for screening of nanoparticle interactions and mechanism(s) of passage across the BBB. In order to conduct the internal benchmarking validation, two teams, each consisting on one postdoctoral researcher and one postgraduate student researcher, were tasked with following the identical protocol for growth of the hCMEC/D3 cell line for 7 days according to the detailed protocol described in the Materials section below. On day 7, the barrier integrity was determined by each team, by calculating the apparent permeability of the barriers using fluorescently labeled dextran. Results were compared to the literature values for this cell line. Once it was clear that both teams could obtain the same barrier strength, significant additional work was performed, using Transmission Electron Microscopy to confirm that monolayers and tight junctions were formed. Preliminary assessments of the passage of fluorescently labeled ApoE protein, as a positive control for receptor-mediated uptake, and 50-nm SiO_2 nanoparticles (NPs) through BBB were also conducted, and some of the challenges associated with this are also discussed in this manuscript.

2. Results and discussion

2.1. Optimization of the barrier growth conditions

In order for the hCMEC/D3 cells to function as a barrier, it is essential that they form a confluent monolayer and tight junctions between the cells, which prevents paracellular (between cells) transport. We have used extensive electron microscopy imaging to characterize the phenotype of the cells and their organization on the transwell filters in advance of the transport assays. Fig. 3 shows an EM image of a confluent hCMEC/D3 cell monolayer, grown on collagen/fibronectin-coated, 0.4-μm transwell filter, and the formation of the tight junction between adjacent cells. The detailed protocol for the preparation of the collagen/fibronectin coating, and the cell growth conditions are given in the Materials and Methods. In contrast to some published methods, growth factor depleted medium is necessary for the formation of the cell monolayer.

2.2. Apparent permeability of the in vitro BBB model

One measure of the "tightness" of the BBB model can be determined as the apparent permeability based on the flux of a molecule of known MW across the barrier (from the apical to the basolateral chambers, as measured by the change in fluorescence). For simple molecules, the fluid flux is linearly proportional to the dose applied, with more substance transport being observed at higher apical doses. However, due to physical and/or chemical factors, nanoparticle interaction with living systems do not often follow this general rule, as in many cases nanoparticle agglomeration increases at higher particle concentrations, and large particle-aggregates are unable to transport across the BBB. Note however that *in vivo*, larger particles or particle-aggregates may be carried across the BBB in macrophages, and indeed this is the transport method utilized by many viruses [13].

The apparent permeability (P_{app}) of the model, grown on the collagen/fibronectin filters into a BBB, was determined as part of the – internal benchmarking process, and the values obtained by the two teams were compared to those in the literature for 4kD fluorescein isothiocyanate-dextran (FD4 kDa). FD4 is used as a marker for paracellular permeability of the endothelial monolayer and has been found to be consistently low in this *in vitro* BBB model, due to the close contact of the hCMEC/D3 cells and their successful functioning as a barrier (8). The values are shown in Fig. 4, and the UCD values sit within the range of literature values. The data also shows the robust nature of the barriers, as the spread of the values for the two UCD teams is small (indicated by the error bars) despite the barriers being prepared at different times. An example of the time-resolved passage of FD4 kDa through the blank filter and the hCMEC/D3 barrier is shown in Fig. 5. The "blank" refers to the transport of FD4 kDa through the filter alone, with no cellular barrier grown on top. It is clear that the small pore size of the filter (0.4 μm) exerts a significant barrier effect hCMEC/D3 monolayer itself, even for the small FD4 kDa molecules, as initially 100 μg of FD4 kDa was applied to the apical side of the transwell and an average of 14 μg FD4 kDa passed through the filter after 2 h. It is also clear that paracellular transport is significantly reduced in the presence of the hCMEC/D3 monolayer as approximately 2.5 μg FD4 kDa was found to bypass the hCMEC/D3 cells after 2 h of exposure.

Quantification of the trans-endothelial electrical resistance (TEER) by this *in vitro* BBB model was carried out as an additional method to evaluate monolayer integrity. As shown in Fig. 6, both teams found TEER values of approximately 40 Ohms by the seventh day of monolayer formation, which is very similar to the published values (8).

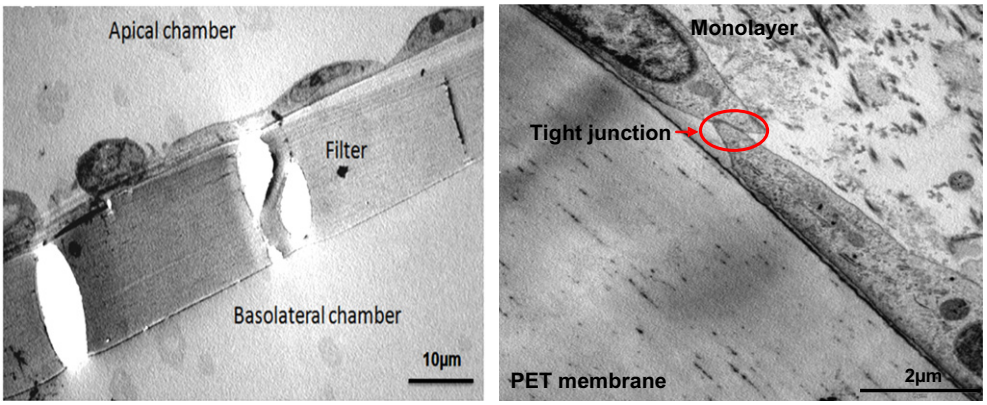

Fig. 3. Electron microscope image of the hCMEC/D3 monolayer grown on a collagen/fibronectin-coated 0.4-μm membrane. The EM image on the left clearly illustrates the growth of a confluent monolayer. On the right, an electron dense tight junction between two adjacent hCMEC/D3 cells can be seen. (For interpretation of the references to colour in this figure legend, the reader is referred to the web version of this article.)

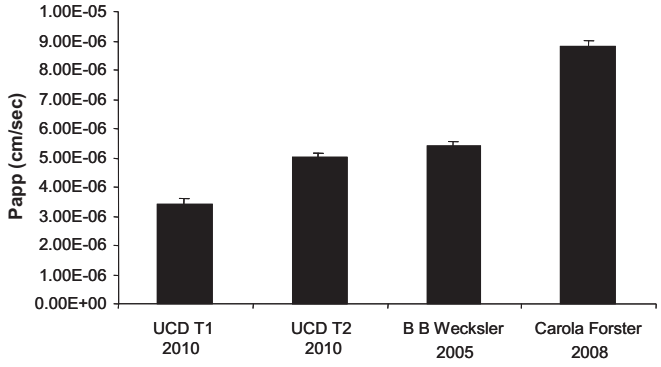

Fig. 4. Comparison of the apparent permeability values of the two teams in the min-RR with the literature values for FD4 kDa. Each of the UCD values are the mean of 12 replicates and the SD is shown, indicating the degree of reproducibility of the barriers. Excellent reproducibility between the two teams is observed, indicating the robustness of the protocol.

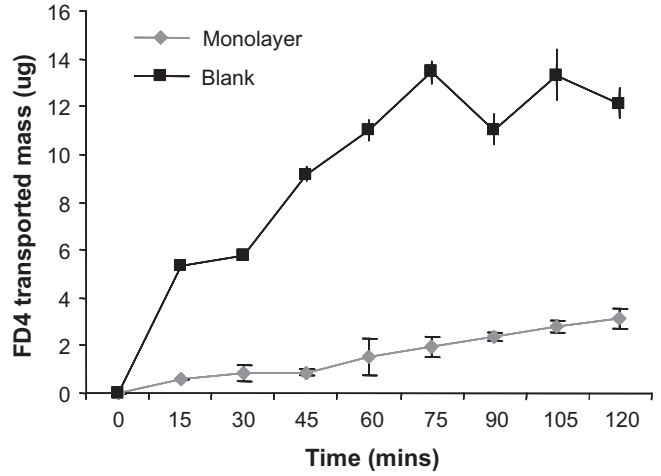

Fig. 5. FD4 kDa transport through the *in vitro* BBB model. Transport of FD4 kDa across the filter alone (blank) and the *in vitro* BBB model (monolayer) as a function of time. An increased flux of FD4 kDa was found through the blank filter membrane compared to the monolayer over 2 h.

2.3. Validation of a transcytosis mechanism through the in vitro BBB model

Despite being designed to keep foreign entities out, there are many transport pathways across the BBB specifically designed to transport essential nutrients (including proteins and lipids) across the BBB, as was shown schematically in Fig. 1. We chose Apolipoprotein E (ApoE) as a positive control for transcellular transport across the BBB *in vitro* model, as it is known to access the brain through a receptor-mediated mechanism and has been shown to enhance the uptake of drugs [10] and nanoparticles into the brain *in vivo* [10]. The transported mass of ApoE across the BBB model was assessed and the values are shown in Fig. 7. These studies confirm that the BBB *in vitro* model is capable of the transcytosis of ApoE in a quantitatively reproducible manner as similar amounts of ApoE transport were found by both teams.

2.4. Preliminary assessment of nanoparticle passage through the model in vitro BBB

2.4.1. Characterization of the NPs

Prior to all studies of nanoparticle interaction with cells, it is essential to characterize the NP dispersion under the conditions in which they will be presented to the cells – i.e. in the assay medium, and for the duration of the exposure. This is necessary in order to understand the dose of NPs that is being presented to cells, as significant agglomeration of the NPs in the assay media would reduce the available NP dose, and if the samples are not prepared in an identical manner for each experiment, the resultant dose could be completely different from experiment to experiment.

Fig. 8 shows the size distribution of the 50-nm SiO_2 nanoparticles in the transport assay medium over the time course of the transport experiments (4 h), determined using dynamic light scattering (DLS). The data in Table 1 also highlights a key limitation of the DLS technique, which is that it gives a mean value, which is actually physically quite meaningless in the presence of multiple peaks such as are observed here. However, for the purpose of our transport assays, the data show that after the initial decrease of the mean peak, the size distribution remains relatively constant over the 4 h of the experiment, suggesting that the available NP dose remains relatively constant throughout the assay.

2.5. Transport of 50-nm SiO_2 nanoparticles through the in vitro BBB model

A key advantage of nanoparticles, which makes them very attractive as potential drug carriers for nanomedicine and nanotherapy, is that nanoparticles also access the endogenous active transport mechanisms of cells, likely as a result of attracting proteins and protein complexes to their surface [3,4], and thereby presenting a biological identity to the cellular membranes [11,12].

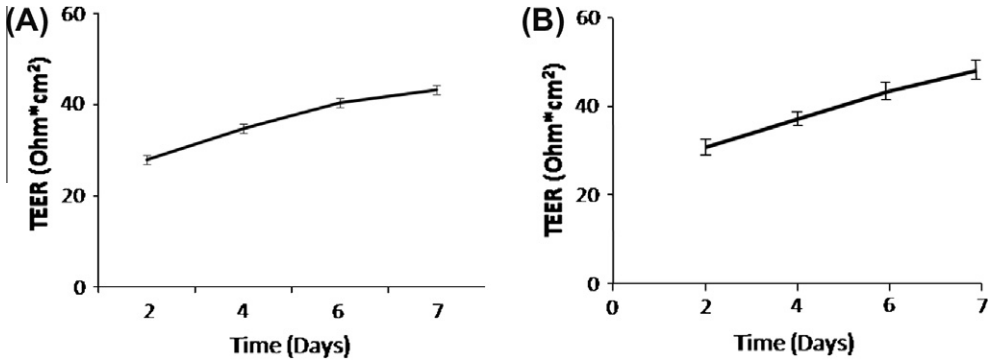

Fig. 6. TEER values of the *in vitro* BBB during the seven days of monolayer growth as reported during the internal benchmarking process. (A&B) Both team 1 and team 2 reported similar TEER values over the BBB culture period, which increase to approximately 40 Ohms. Two-way ANOVA showed no significant difference between T1 and T2 TEER measurements over time.

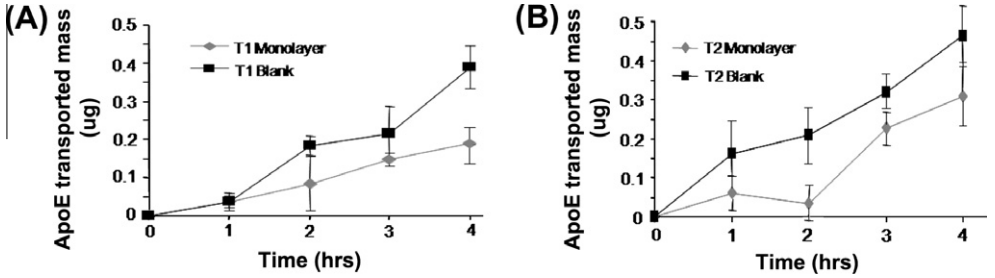

Fig. 7. Comparison of ApoE transport through the *in vitro* BBB during internal benchmarking study. The transport of ApoE was found to be reproducible through both the monolayer and the blank filter membrane (Data are mean ± std, $3 \leqslant n \leqslant 6$. Two-way ANOVA showed no significant differences of ApoE transport upon comparison of T1 versus T2 between monolayer or blank values over time).

Thus, in analogy with the transport data for the positive control protein (ApoE), we expect that the transport of the 50-nm SiO_2 NPs should also be significantly different in the presence and absence of cellular energy.

Transport assays for green-fluorescent 50-nm SiO_2 NPs, presented to the apical chamber at a concentration of 100 μg/mL, were performed by the two teams as the final step in the internal benchmarking process. One should be critical of several aspects of these conditions. Firstly, dye leakage has been found to be a highly significant element in uptake studies within our laboratory, and given the small amounts of transport involved here, an even more serious issue. Indeed, several explorations with a variety of commercially available labeled nanoparticles indicate that most of the apparent transport derives from leeching dye across the barrier [18]. One should also note the rather high doses used in this study (to increase the signal-to-noise ratio), and this undesirable element of such studies should in future be addressed.

The transport of the 50-nm SiO_2 NPs across the BBB, under the normal tissue culture conditions, when the cellular process are occurring normally, is reduced to ~50% of the values in the absence of the cell layer (the blank filter alone), suggesting that the cellular monolayer is acting to prevent the NPs from equilibrating across the BBB, and that some active transport of NPs across the BBB is occurring, as shown in Fig. 9A and B. In addition, the 50-nm SiO_2

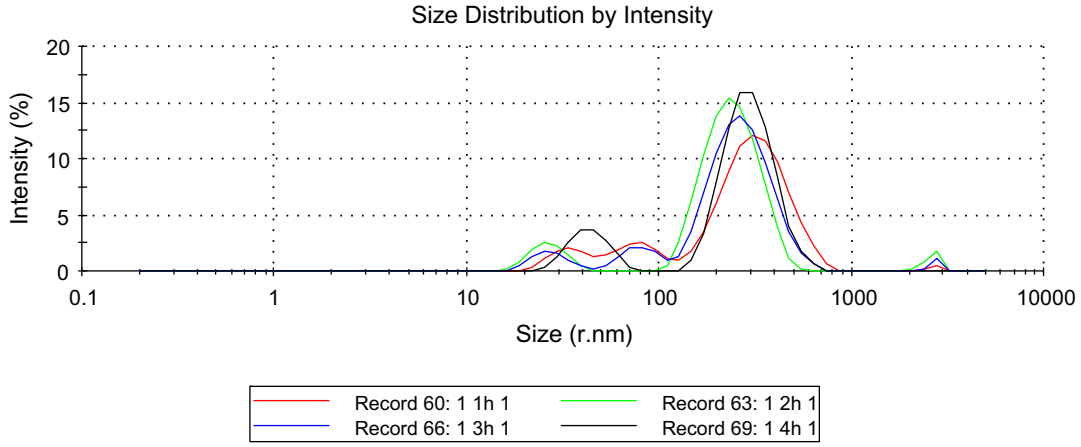

Fig. 8. DLS plots of the size distribution of nominally 50-nm SiO_2 NPs dispersed in transport assay medium at 1-h increments following the preparation of the initial dispersion. (For interpretation of the references to colour in this figure legend, the reader is referred to the web version of this article.)

Table 1
Detailed description of the average size of the nominally 50-nm SiO_2 NPs dispersed in the transport assay medium, at 1-h increments following the preparation of the initial dispersion. Some agglomeration and polydispersity of the 50-nm SiO_2 NPs was found upon incubation in assay medium at 37 °C over 4 h. This was attributed to the interaction of the 50-nm SiO_2 NPs with proteins within the assay medium.

Sample time (h)	Z aver (dnm)	Peak 1 (nm)	% Intensity	PDI	Width (nm)	Attn
1	175.0	334.4	77.9	0.632	123.0	7
2	185.1	247.4	88.0	0.576	77.12	7
3	189.6	279.9	83.4	0.569	99.38	7
4	201.7	304.0	84.4	0.623	91.91	7

NPs did not reach equilibrium within the blank transwell as 4 h after exposure of 50-nm SiO_2 NPs to the apical chamber approximately 7% of the original dose had crossed the 0.4 μm filter, as read by the level of fluorescence in the basal chamber. This may be due to a combination of 50-nm SiO_2 NPs agglomeration to ~200 nm in the assay medium and the nonlinear shape of the 0.4 μm pores within the filter membrane. Ongoing optimizations of these models will be necessary to investigate the detailed mechanism of 50-nm SiO_2 NPs passage through the model BBB, and in particular to reduce the influence of the filter membrane, while maintaining the cellular barrier reproducibility. These are somewhat opposing needs in practice, in our experience.

As FD4 kDa was used previously as a marker of paracellular permeability, ApoE was used in this case as a marker for receptor-mediated transcytosis through the hCMEC/D3 cell monolayer. The percentage transported mass of ApoE after 4 h was ~40% of the original exposure dose (Fig. 10). This is perhaps unsurprising as it has been reported that ApoE can enter the brain through the bloodstream. Approximately 7% of the 50-nm SiO_2 NPs exposure dose crossed the monolayer and the initial high exposure dose of 100 μg/ml highlights the robust properties of this cell line to impede the transport of foreign molecules. The exact mechanism of transport is as yet unknown; however, it has been shown that a protein corona surrounds nanoparticles in physiological medium and these proteins guide the nanoparticle–cell interaction. Further investigation into the exact corona formed on 50-nm SiO_2 NPs in assay media will be instructive on this matter.

In order to confirm visually that the 50-nm SiO_2 NPs were being transported through the hCMEC/D3 monolayer, an electron microscopy study was performed on the same timescale (4 h) and under identical conditions as the transport studies in order to track the passage of the nanoparticles. The full details of this time-resolved mechanistic study will be reported separately, but some representative images are shown here as confirmation of a transcellular mechanism. Fig. 11 shows a series of EM images of hCMEC/D3 cells grown on collagen/fibronectin-coated transwell filters (0.4 μm pore size) exposed to 100 μg/ml 50-nm SiO_2 NPs for 1 h. In Fig. 10A, uptake can be observed as the plasma membrane envelopes the 50-nm SiO_2. In Fig. 10B, the SiO_2 NPs can be observed in endosomes and lysosomes, and a nanoparticle can be observed on the basolateral side of the cell which is suggestive of an exocytosis process, whereby the particles are released from the basolateral side of the cell. In Fig. 12, a small number of 50-nm SiO_2 NPs can be seen adhering to the pore of the blank PET membrane 4 h post NP exposure. Various other filter membranes are currently under investigation to circumvent this issue.

3. Materials and methods

3.1. Cell culture

Immortalized human brain capillary endothelial cells (hCMEC/D3) were obtained from Florence Miller, B.B. Wecksler (Inserm, France). The original brain endothelial cells were isolated from human brain tissue following surgical excision of an area of the temporal lobe of an adult female with epilepsy. The hCMEC/D3 cell line was formed by immortalization of the aforementioned endothelial cells by lentiviral transduction of the catalytic subunit of human telomerase and SV40-T antigen (8). The hCMEC/D3 cells were used from passage 7–10. For culturing, 50,000 cells were seeded in a collagen-coated flask (25 cm^3, Becton Dickinson) and supplemented with EBM-2 medium containing vascular endothelial growth factor (VEGF), insulin-like growth factor-1 (IL-1), epidermal growth factor (EGF), basic fibroblast growth factor (bFGF), fetal calf serum (2%), gentamicin sulphate/amphotericin B and hydrocortisone (Lonza Biosciences). For migration assays, cells were supplemented with growth factor depleted EBM-2 assay medium containing bFGF, 2% FCS, hydrocortisone and 10 mM HEPES during monolayer formation. Cells were cultured in an incubator at 37 °C with 5% CO_2/95% air and saturated humidity. Cell culture medium was changed every two days and monolayer medium twice weekly.

3.2. Transport assays and P_{app} determination

The *in vitro* BBB system was prepared on a 12-well format on a PET membrane transwell (1.12 cm^2, 0.4 μm pore size, Corning). Membrane inserts were coated with 200 μl collagen/fibronectin (15% rat tail collagen and 15% bovine fibronectin, Invitrogen) 1 day prior to use and stored at 37 °C in a dry incubator. For transport experiments, hCMEC/D3 cells were seeded in 500 μl assay media at a density of 5×10^5 cells per 1.2-cm^2 filter in the apical compartment and 1500 μl assay media in the basolateral compartment. Assay medium was changed twice weekly. Transport assays were conducted 7–10 after seeding. Both the apical and basolateral chambers were washed twice with assay medium directly before

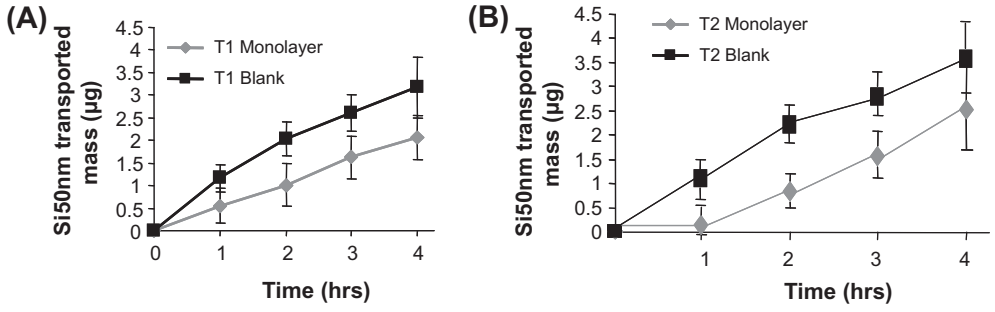

Fig. 9. Comparison of SiO_2 50 nm NPs transport assays over 4 h. Similar transported mass values through the *in vitro* BBB model were obtained for both teams within the internal benchmarking study showing the reproducibility of the BBB monolayer in the study of nanoparticle uptake (Data are mean ± std, $3 \leqslant n \leqslant 6$. Two-way ANOVA showed no significant differences of 50-nm SiO_2 transport upon comparison of T1 versus T2 monolayer or blank values over time).

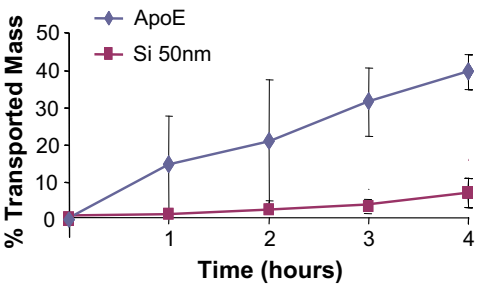

Fig. 10. Percentage transported mass of 50-nm SiO_2 NPs and ApoE transcytosis control. A higher percentage of ApoE was found to cross the BBB monolayer compared to 50-nm SiO_2 NPs ($3 \leqslant n \leqslant 6$). (For interpretation of the references to colour in this figure legend, the reader is referred to the web version of this article.)

experiments began. Monolayers were used for migration assays 7–10 day's post-transwell seeding. Transport study set-up involved a 500 μl assay medium application to the transwell apical compartment containing FD4 kDa (200 μg/ml), silica nanoparticles (50 nm, 100 μg/ml) or ApoE (1.98 μg/ml), respectively. The basolateral compartment contained 1500 μl assay medium and transwells were placed in an orbital shaker at 37 °C. Samples of 100 μl assay medium were removed from the basolateral compartment every 15 min in the case of FD4 kDa and every 1 h for ApoE and 50-nm SiO_2 NPs and aliquoted onto black flat-bottomed 96-well plates. The 100 μl sample was replaced with assay medium after each sampling. The fluorescence of FD4 kDa, ApoE and 50-nm SiO_2 NPs was determined using a fluorimeter with an excitation/emission wavelength of 490 nm/515 nm for FD4, 485 nm/514 nm 50-nm SiO_2 NPs and 650 nm/668 nm for ApoE. A standard curve of fluorescence was calculated for each molecule in order to determine sample concentration. The apparent permeability (P_{app}) was calculated according to the method of Artursson (1990) using the following equation:

$$P_{app} = dQ/dt * 1/A * C_o * 60$$

where dQ/dt is the amount of FD4 kDa, 50-nm SiO_2 NPs or ApoE transported per minute (ng/min), A is the surface area of the filter (cm^2), C_o is the initial concentration of FD4 kDa, 50-nm SiO_2 NPs or ApoE and 60 is the conversion from minutes to seconds.

3.3. Transmission electron microscopy

Seven-day-old hCMEC/D3 monolayers were exposed to 100 μg/mL 50-nm SiO_2 NPs in an orbital shaker (100 rpm) for 1 h at 37 °C. Permeable filters containing a confluent monolayer of endothelial cells were fixed with glutaraldehyde (2.5%, v/v) in Sorensen phosphate buffer for 1 h at room temperature, and post-fixed with osmium tetroxide (1%, w/v) in de-ionized water for 1 h. After dehydratation in a graded series of 70%, 90%, and 100% ethanol and embedding in epoxy resin, sections were cut perpendicular to the monolayer with a Leica Microtome, contrasted with 2% uranyl acetate and lead citrate, and examined with an electron microscope (TECNAI).

3.4. Nanoparticle dispersion and characterization

50-nm SiO_2 NPs were purchased from Kisker-biotech. The size of the 50-nm SiO_2 NPs dispersed in assay media was determined

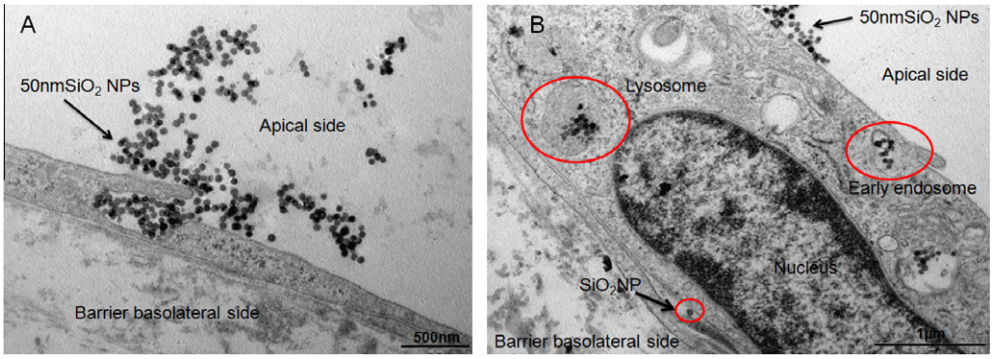

Fig. 11. EM images of transport of 50-nm SiO_2 NPs through the hCMEC/D3 monolayer 4 h post-exposure. Scale bars are 500 nm and 1 μm respectively. Uptake of 50-nm SiO_2 NPs by the plasma membrane was visualized in the hCMEC/D3 monolayer. The image on the right depicts localization of 50-nm SiO_2 NPs within a polarized hCMEC/D3 cell. (For interpretation of the references to colour in this figure legend, the reader is referred to the web version of this article.)

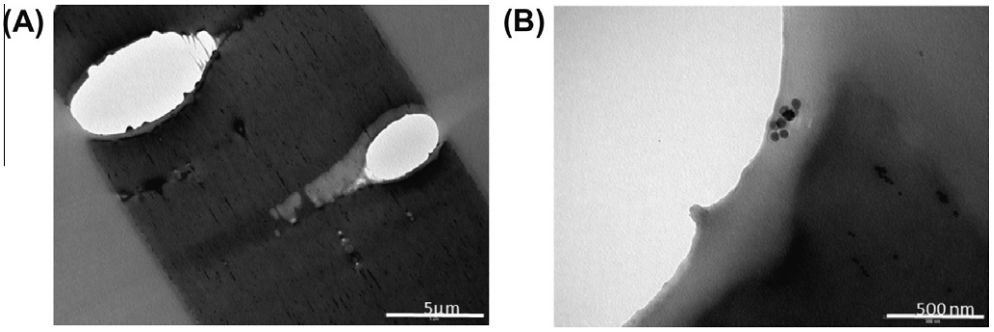

Fig. 12. EM images of transport of 50-nm SiO_2 NPs through the PET filter membrane 4 h post-exposure. Scale bars are 5 μm and 500 nm respectively. (A) The image on the left depicts an overview of the 0.4-μm blank PET membrane post-exposure to 50-nm SiO_2 NPs. (B) Magnified image of a single PET membrane pore with a number of 50-nm SiO_2 NPs adhering to the pore surface.

with a Malvern Zetasizer 3000HSa. The particles were diluted in 1.5 ml assay medium to reach a 100 μg/ml concentration. The solution of particles was incubated at 37 °C in an orbital shaker over 4 h and sampled each hour. The measurements were conducted at 37 °C by transferring 500 μL of the stock solution to a square cuvette for DLS analysis. DLS analyzes the velocity distribution of particle movement by measuring dynamic fluctuations of light-scattering intensity caused by the Brownian motion of the particle. This technique yields a hydrodynamic radius, or diameter, to be calculated via the Stokes–Einstein equation from the aforementioned measurements.

3.5. Statistical analysis

Statistical analysis was carried out by 2-Way ANOVA and Bonferroni post-test on transport studies both of 50-nm SiO_2 NPs and ApoE, as well as on the TEER measurements (GraphPad Prism 4.0). A *p*-value of less than 0.05 was deemed significant.

4. Conclusions

By careful application of a robust protocol, it has been possible to obtain quantitatively reproducible results across two teams regarding the transport of a simple macromolecule (FD4 kDa), a known brain transporter protein (ApoE) through a *in vitro* BBB model based on hCMEC/D3 cells which form a monolayer and tight junctions when grown on transwell filters coated with collagen/fibronectin. This internal benchmarking validation of the *in vitro* BBB model confirmed the formation of the *in vitro* BBB and the appropriate functioning of a receptor-mediated transport mechanism, based on the transport of the positive control ApoE shown by each team. Having validated the hCMEC/D3 BBB model, preliminary studies using fluorescently labeled 50-nm SiO_2 NPs were performed by the two teams, again with excellent reproducibility and agreement. However, these studies, while showing promise (in particular in their reproducibility) nanoparticle (50 nm SiO_2) transport remains less compelling, in particular due to limitations of pore–particle interactions. In all cases, the pore size of the transwell filter was 0.4 μm, which although significantly larger than the nanoparticles, did impact on the transport across the filter, and the effect from the filter was quite large relative to the impact of the hCMEC/D3 cell monolayer. However, EM imaging confirms the NP transport is via a transcellular process. Time-resolved mechanistic work is underway and will be reported separately. We emphasize that if indeed the particles are passing through the cells, then this is significant. It suggests that such models do seem to enable a true transcytosis-based mechanism for nanoparticle BBB crossing and justifies further investment in them in future.

More recent work in our laboratory has been carried out, repeating this work using a transwell filter with 3-μm pores. After considerable efforts, the cell has been shown to develop its function and resulted in a significant alteration in the amount of nanoparticles crossing the barrier in the presence of the hCMEC/D3 cell monolayer, relative to the amount of nanoparticles crossing the blank filter alone.

Other support geometries are also being explored, as well as a variety of different imaging and other molecular biology tools to study the BBB system. While we cannot be sure if these systems will represent a robust screening tool for nanoparticles crossing into the brain, we feel there is sufficient hope that they may be able to rank in order efficiency in terms of nanoparticle characteristics (e.g. size, shape, surface charge, biological identity (protein or biomolecule corona)) and to investigate the mechanism(s) utilized by nanoparticles to cross the BBB.

Acknowledgements

This research has been supported by EPA STRIVE Fellowship, 2008-EH-MS-5-S3 (M. Brown, M.N.R.), by the EU FP7 Small Collaborative project NeuroNano, NNP4-SL-2008-214547 (M.N.R., M. Bramini), and by an ESF EpitopeMap Research Networking Programme Exchange grant (M. Bramini). Part of this work was conducted under the framework of the INSPIRE Programme, funded by the Irish Government's Programme for Research in Third Level Institutions, Cycle 4, National Development Plan 2007–2013 (DY). The SFI SRC BioNanoInteract (07 SRC B1155) also supported part of the research reported here. Use of the UCD Electron Microscopy Core facility is also acknowledged.

References

[1] M.A. Dobrovolskaia, S.E. McNeil, Nat. Nanotechnol. 2 (8) (2007) 469–478.
[2] N.J. Abbott, L. Ronnback, E. Hansson, Nat. Rev. Neurosci. 7 (1) (2006) 41–53.
[3] T. Cedervall, I. Lynch, M. Foy, T. Berggård, S.C. Donnelly, G. Cagney, S. Linse, K.A. Dawson, Angew. Chem. Int. Ed. 46 (2007) 5754–5756.
[4] E. Hellstrand, I. Lynch, A. Andersson, T. Drakenberg, B. Dahlbäck, K.A. Dawson, S. Linse, T. Cedervall, FEBS J. 276 (2009) 3372–3381.
[5] L. Juillerat-Jeanneret, Drug Discov. Today 13 (23–24) (2008) 1099–1106.
[6] N.F. Fletcher, D.J. Brayden, B. Brankin, S. Worrall, J.J. Callanan, Vet. Immunol. Immunopathol. 109 (3–4) (2006) 233–244.
[7] B. Poller, H. Gutmann, S. Krahenbuhl, B. Weksler, I. Romero, P.O. Couraud, G. Tuffin, J. Drewe, J. Huwyler, J. Neurochem. 107 (5) (2008) 1358–1368.
[8] B.B. Weksler, E.A. Subileau, N. Perriere, P. Charneau, K. Holloway, M. Leveque, H. Tricoire-Leignel, A. Nicotra, S. Bourdoulous, P. Turowski, D.K. Male, F. Roux, J. Greenwood, I.A. Romero, P.O. Couraud, FASEB J. 19 (13) (2005) 1872–1874.
[9] M.L. Chapagain, S. Verma, F. Mercier, R. Yanagihara, V.R. Nerurkar, Virology 364 (1) (2007) 55–63.
[10] K. Michaelis, M.M. Hoffmann, S. Dreis, E. Herbert, R.N. Alyautdin, M. Michaelis, J. Kreuter, K. Langer, J. Pharm. 317 (2006) 1246–1253.
[11] I. Lynch, A. Salvati, K.A. Dawson, Nat. Nanotechnol. 4 (2009) 546–547.
[12] D. Walczyk, F. Baldelli-Bombelli, A. Campbell, I. Lynch, K.A. Dawson, JACS 132 (2010) 5761–5768.
[13] L.M. Dallasta, L.A. Pisarov, J.E. Esplen, J.V. Werely, A.V. Moses, J.A. Nelson, Am. J. Pathol. 155 (1999) 1915–1927.
[14] M. Lundqvist, J. Stigler, T. Cedervall, G. Elia, I. Lynch, K.A. Dawson, PNAS 105 (2008) 14265–14270.
[15] G. Oberdörster, A. Elder, A. Rinderknecht, J. Nanosci. Nanotechnol. 9 (8) (2009) 4996–5007.
[16] S. Bhaskar, F. Tian, T. Stoeger, W. Kreyling, J.M. de la Fuente, V. Grazú, P. Borm, G. Estrada, V. Ntziachristos, D. Razansky, Part. Fibre Toxicol. 7 (2010) 3.
[17] A. Zensi, D. Begley, C. Pontikis, C. Legros, L. Mihoreanu, C. Büchel, J. Kreuter, J. Drug Target. 18 (10) (2010) 842–848.
[18] A. Salvati, T. Dos Santos, J. Varela, C. Åberg, P. Pinto, I. Lynch, K.A. Dawson, Experimental and theoretical approach to comparative nanoparticle and small molecule intracellular import, trafficking, and export, nanomedicine, in press.
[19] B. Rothen-Rutishauser, C. Mühlfeld, F. Blank, C. Musso, P. Gehr, Part. Fibre Toxicol. 4 (2007) 9.
[20] S. Diabaté, S. Mülhopt, H.R. Paur, H.F. Krug, Altern. Lab. Anim. 36 (2008) 285–298.